View metadata, citation and similar papers at core.ac.uk
brought to you by CORE
provided by CiteSeerX

PHYSICAL REVIEW B **79**, 245202 (2009)

Electronic structure and phase stability of MgTe, ZnTe, CdTe, and their alloys in the *B*3, *B*4, and *B*8 structures

Ji-Hui Yang, Shiyou Chen, Wan-Jian Yin, and X. G. Gong
Department of Physics and MOE Laboratory for Computational Physical Sciences, Fudan University, Shanghai 200433, People's Republic of China

Aron Walsh and Su-Huai Wei
National Renewable Energy Laboratory, Golden, Colorado 80401, USA
(Received 25 March 2009; published 2 June 2009)

The electronic structure and phase stability of MgTe, ZnTe, and CdTe were examined in the zinc-blende (*B*3), wurtzite (*B*4), and NiAs-type (*B*8) crystal structures using a first-principles method. Both the band-gap and valence-band maximum (VBM) deformation potentials of MgTe, ZnTe, and CdTe in the *B*3 structure were analyzed, revealing a less negative band-gap deformation potential from ZnTe to MgTe to CdTe, with a VBM deformation potential increase from CdTe to ZnTe to MgTe. The natural band offsets were calculated taking into account the core-level deformation. Ternary alloy formation was explored through application of the special quasirandom structure method. The *B*3 structure is found to be stable over all (Zn,Cd)Te compositions, as expected from the preferences of ZnTe and CdTe. However, the (Mg,Zn)Te alloy undergoes a *B*3 to *B*4 transition above 88% Mg concentration and a *B*4 to *B*8 transition above 95% Mg concentration. For (Mg,Cd)Te, a *B*3 to *B*4 transition is predicted above 80% Mg content and a *B*4 to *B*8 transition above 90% Mg concentration. Using the calculated band-gap bowing parameters, the *B*3 (Mg,Zn)Te [(Mg,Cd)Te] alloys are predicted to have accessible direct band gaps in the range 2.39(1.48)–3.25(3.02) eV, suitable for photovoltaic absorbers.

DOI: 10.1103/PhysRevB.79.245202 PACS number(s): 71.20.Nr, 71.23.An, 71.55.Gs, 78.55.Et

I. INTRODUCTION

Multiternary semiconductor alloys are essential components in both existing and next-generation optoelectronic devices such as solar cells, as they offer great flexibility in tuning emission and absorption wavelengths and controlling lattice constants.[1–8] Experimentally, MgTe, ZnTe, and CdTe are found to have room-temperature direct band gaps of 3.5, 2.4, and 1.5 eV, respectively.[9] This makes them excellent candidates for low-cost thin film or high efficiency multijunction solar cell materials to complement existing CdTe and Cu(In,Ga)Se_2 technologies.[10–12] Their potential for high efficiency solid-state light-emission devices has also been noted.[13,14]

Despite the small lattice mismatch between MgTe and CdTe (less than 1%), and the relatively small atomic size and chemical mismatch between Mg and Zn, alloy formation in this system is expected to be structurally complex. This originates from the ground-state structural preferences of the binary tellurides. ZnTe and CdTe adopt tetrahedral coordination in the cubic zinc-blende (*B*3) structure ($F\bar{4}3m$). Experimentally MgTe is reported to favor the wurtzite (*B*4) structure ($P6_3mc$),[15–17] while theoretically MgTe is predicted to be more stable in the NiAs-type (*B*8) structure ($P6_3mmc$).[18,19] However, experimentally at relatively low pressures (1–3.5 GPa), a *B*4 to *B*8 transition is observed for MgTe, and it has been suggested that the *B*4 structure may be a high-temperature metastable phase, with the *B*8 structure being the true thermodynamic ground state, in agreement with theory.[20]

In the *B*3 crystal structure, the anions form an ideal fcc array, with cation occupying half of the tetrahedral holes. In the *B*4 structure, the anion stacking becomes a hcp array, with reduced C_{3v} site symmetry. However, the fourfold local coordination in both the *B*3 and *B*4 polymorphs is similar. For MgTe the *B*3 structure lies slightly higher in energy due to its smaller Madelung constant. In contrast, the hexagonal *B*8 structure features a hcp anion sublattice with cations occupying the octahedral holes [the hexagonal analog of the cubic NaCl (B1) crystal structure], Fig. 1. As a result of this mismatch in cation coordination preferences, alloys formed from MgTe, ZnTe, and CdTe exhibit a sensitive structure-composition dependence, with *B*3, *B*4, and *B*8 crystals predicted at various alloy compositions. Knowledge of the electronic structure and band alignment of these binary tellurides in each polymorph is therefore very important for understanding the alloy properties and addressing their potential for solar-cell applications. Furthermore, as MgTe, ZnTe, and CdTe in the *B*8 structure all possess indirect band gaps, formation of NiAs-type alloys will be highly undesirable for optoelectronics use and should be avoided.

To obtain a rigorous understanding of the relationship between the geometric and electronic structure, we have performed first-principles calculations and detailed electronic-structure analysis of MgTe, ZnTe, and CdTe in the binary *B*3,

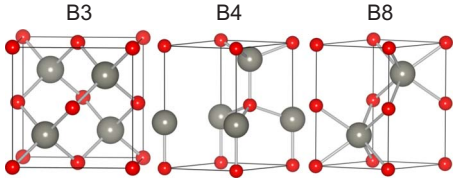

FIG. 1. (Color online) Conventional unit cells of the zinc-blende (*B*3), wurtzite (*B*4), and NiAs-type (*B*8) structures.

 ©2009 The American Physical Society

*B*4, and *B*8 structures. The band-gap and valence-band maximum (VBM) deformation potentials were analyzed in the *B*3 structure, showing that the band-gap deformation potentials at the Γ point become less negative from ZnTe to MgTe to CdTe, while the VBM absolute volume-deformation (VD) potentials increase from CdTe to MgTe to ZnTe. The natural valence-band offsets between the three semiconductor compounds were calculated taking into account the core-level deformation contributions. The properties of random ternary alloys were also studied, including calculation of the band-gap bowing parameters and analysis of the formation energies and phase stability. Our results are compared to previous predictions and available experimental data. Based on this work, we estimate that the *B*3 structure is stable over all (Zn,Cd)Te compositions as expected from the preferences of the binary tellurides. The (Mg,Zn)Te alloy undergoes a *B*3 to *B*4 transition above 88% Mg content and a *B*4 to *B*8 transition above 95% Mg content. For (Mg,Cd)Te, a *B*3 to *B*4 transition is predicted above 80% Mg concentration, with a *B*4 to *B*8 transition above 90% Mg.

II. CALCULATION METHODS

Calculations were performed using density-functional theory (DFT) (Refs. 21 and 22) based on the local-density approximation (LDA),[23] as implemented in the VASP code.[24,25] The electron and core interactions are included using the frozen-core projector augmented wave approach.[26] The shallow-core Zn 3*d* and Cd 4*d* states are explicitly treated as valence electrons. The cutoff kinetic energy for the plane-wave basis wave functions is chosen as 300 eV for all the calculations. The Monkhorst-Pack *k*-point meshes[27] of $9\times9\times9$ for the *B*3 binary structure and $12\times12\times6$ for the *B*4 and *B*8 structures were employed. The bulk binary structures were each optimized to their equilibrium volume through minimization of the total energy and stress. The bulk moduli (B) were obtained through a fit of the energy-volume data to the Murnaghan equation of state.[28] The band-gap volume-deformation potentials (α_V) were obtained from the relation

$$\alpha_V = \frac{\partial E_g}{\partial \ln V} \tag{1}$$

while the pressure-deformation potentials (α_P) were obtained through the application of the bulk modulus

$$\alpha_P = -\left(\frac{1}{B}\right)\alpha_V. \tag{2}$$

For the determination of the band alignments of II-VI semiconductor compounds, only the *B*3 structure was explicitly considered. To calculate the "natural" valence-band offsets between two binary semiconductors *AX* and *BY* at their equilibrium lattice constants, we first calculate the band offsets when the two compounds are in their averaged lattice constant using the approach similar to that used in core-level x-ray photoemission spectroscopy,[29,30] that is

$$\Delta E_v^{(\mathrm{av})}(AX/BY) = \Delta E_{v,\mathrm{core}}^{(\mathrm{av})}(AX/BY) + \Delta E_{C,C'}^{(\mathrm{av})}(AX/BY), \tag{3}$$

where

$$\Delta E_{v,\mathrm{core}}^{(\mathrm{av})}(AX/BY) = \Delta E_{v,C'}^{(\mathrm{av})}(BY) - \Delta E_{v,C}^{(\mathrm{av})}(AX). \tag{4}$$

Here $\Delta E_{v,C}^{(\mathrm{av})}(AX)=E_v^{(\mathrm{av})}(AX)-E_C^{(\mathrm{av})}(AX)$ [the same for $\Delta E_{v,C'}^{(\mathrm{av})}(BY)$], which is the energy difference between the VBM and core level at the average lattice constant. $\Delta E_{C,C'}^{(\mathrm{av})}(AX/BY)=E_{C'}^{(\mathrm{av})}(BY)-E_C^{(\mathrm{av})}(AX)$ is the energy difference between the two core levels, which can be obtained through a calculation for the unrelaxed $(AX)_n/(BY)_n$ superlattice at the average lattice constant. After $\Delta E_v^{(\mathrm{av})}(AX/BY)$ is obtained using the above procedure, the shift of the VBM states $a_{\mathrm{VBM}}\frac{\Delta V}{V}$ from the averaged lattice constant to equilibrium lattice constant for the binary compounds *AX* and *BY* arising from the VBM absolute volume-deformation potentials[31,32] are added to get the final natural band offset $\Delta E_v(AX/BY)$. This approach thus provides a more accurate way to calculate the natural band offsets without making assumptions to the deformation potential of core levels or other reference states.[30]

The ternary random alloys $A_xB_{1-x}Te$ were modeled within 64-atom (32-mixed cation) supercells using the special quasirandom structure (SQS) approach[33,34] to determine the cation-site occupancies. The cubic *B*3 structural alloys are constructed with ideal lattice constants $2a$ and the *B*4 and *B*8 structured alloys are represented through orthorhombic cells with ideal lattice constants of $2a$, $2\sqrt{3}a$, and $2\sqrt{8/3}a$. These SQS structures are constructed so that the physically most relevant atom-atom correlation functions approach those of random alloys. We assume that the alloys obey Vegard's law,[35] i.e., the alloy lattice constants are determined by a weighted average of its constituents. The internal atomic positions inside the SQS supercells were fully relaxed through minimization of the quantum-mechanical force on each atom to be below 0.02 eV/Å. The *k*-point meshes for the SQS structures were tested to ensure good precision when comparing the total energies. For the *B*3 structure, $3\times3\times3$ *k*-point meshes were employed and for the *B*4 and *B*8 structures, $4\times2\times2$ *k*-point meshes were employed. The total energy was converged to within 0.5 meV/2-atom for *B*3 and *B*4 supercells and 1 meV/2-atom for the *B*8 supercells.

III. BINARY *B*3, *B*4, AND *B*8 POLYMORPHS

A. Structural properties

The calculated ground states of MgTe, ZnTe, and CdTe are in the *B*8, *B*3, and *B*3 structures, respectively. The LDA-calculated *B*3, *B*4, and *B*8 structural parameters and some experimental parameters, and energy differences per atom for MgTe, ZnTe, and CdTe are listed in Table I. For ZnTe and CdTe, the calculations reproduce the thermodynamically stable phases and are in good agreement with experiment[9] and previous theoretical studies.[18,19,36,37] For MgTe, our calculations did show that MgTe in the *B*4 structure is more stable than in the *B*3 structure and we also found that MgTe

TABLE I. LDA-calculated equilibrium structural properties and electronic band gaps. For the *B*8 structure, MgTe has an indirect band gap (0.74 eV) between the Γ point and the *K* point. *B*8 phases of ZnTe and CdTe have indirect negative band gaps. The relative total-energy difference ΔE is given with respect to the most stable phase for each compound. Available experimental values (Ref. 9) are also presented in parentheses.

	Phase	a (Å)	c/a	u	ΔE (meV/atom)	B (Kbar)	$E_g^{\Gamma-\Gamma}$ (eV)
MgTe	*B*3	6.380(6.414)			19.5	390(376)	2.38(3.49)
	*B*4	4.514(4.530)	1.627(1.635)	0.376	18	391	2.44
	*B*8	4.140	1.630		0	531	2.03
ZnTe	*B*3	6.002(6.089)			0	554(528)	1.30(2.35)
	*B*4	4.234	1.648	0.373	6	553	1.32
	*B*8	3.956	1.659		265	701	0.69
CdTe	*B*3	6.421(6.482)			0	460(422)	0.63(1.48)
	*B*4	4.536	1.642	0.374	4	462	0.67
	*B*8	4.195	1.664		143	608	0.14

in the *B*8 structure is the ground state in agreement with the work of Yeh *et al.*[18,19]

The equilibrium lattice constants of MgTe and CdTe are almost matched. The lattice constant of ZnTe is about 5% smaller than MgTe and CdTe. In the *B*4 and *B*8 structures, the c/a ratios for all of three binary tellurides deviate very little from the ideal value of $\sqrt{8/3}=1.633$. The lattice constants in the *B*8 structure are about 10% smaller than those in the *B*4 structure as to keep the bond lengths similar with sixfold coordination around every atom. The bulk moduli are always much larger for the *B*8 structures due to its smaller volume, with the *B*3 and *B*4 values almost identical for each compound.

B. Electronic band gaps

The calculated band-gap energies are underestimated by the LDA. In the *B*3 structure, the direct band gaps of 2.38, 1.30, and 0.63 eV for MgTe, ZnTe, and CdTe, respectively, relate to the room-temperature experimental gaps of 3.49, 2.35, and 1.48 eV.[9] The band gap of MgTe is larger than that of ZnTe because the *s* state of Mg is higher than that of Zn (Table II) so the conduction band minimum (CBM) of MgTe is higher than that of ZnTe. Another reason is that in ZnTe anion *p*-cation *d* coupling will push its VBM higher. ZnTe has a larger band gap than CdTe due to its smaller lattice constant and shorter bond length. The band gaps of the *B*4 structure are slightly higher than that of the *B*3 structure due to increased level repulsion between the valence and the conduction states in the reduced symmetry *B*4 structure.[38] For the *B*8 structure, MgTe was found to have its VBM at Γ and CBM at *K*, so it has an indirect gap of 0.74 eV. The *B*8 phases of ZnTe and CdTe were also found to have indirect gaps with the VBM occurring along the Γ-*M* line (due to *p*-*d* coupling away from the zone center) and the CBM at the *K* point. We notice that although the LDA calculations underestimate the band gap, the calculated general trends are correct.

TABLE II. LDA-calculated atomic valence electronic eigenvalues ε_s, ε_p, and ε_d (in eV) of related elements.

Atom	ε_s	ε_p	ε_d
Mg	−4.76	−1.35	
Zn	−6.20	−1.22	−10.40
Cd	−5.80	−1.31	−11.75
Te	−15.27	−6.07	−43.48

C. Band-gap deformation potentials

The calculated band-gap volume and pressure-deformation potentials, $\alpha_V^{\Gamma-\Gamma}$ and $\alpha_P^{\Gamma-\Gamma}$, respectively, are listed in Table III. For the *B*3 phase, $\alpha_V^{\Gamma-\Gamma}$ is always negative and it becomes less negative on transition from ZnTe to MgTe to CdTe. In general for the valence band, anion *p*-cation *p* coupling results in a strong positive volume-deformation term, which is partially offset by kinetic-energy contributions and also by anion *p*-cation *d* coupling when shallow *d* states are present (as for Zn and Cd).[39] For the conduction band, the antibonding anion *s*-cation *s* repulsion and kinetic-energy effects usually have a strong negative contribution. These level repulsions decrease as the bond length increases. This explains why the magnitude of $\alpha_V^{\Gamma-\Gamma}$ decreases as the lattice constant increases from ZnTe to MgTe to CdTe. We also find that for the *B*3 phase, $\alpha_V^{\Gamma-X}$ is

TABLE III. LDA band-gap volume-deformation potentials α_V (in eV) and pressure coefficients α_P (in meV/Kbar).

	Phase	$\alpha_V^{\Gamma-\Gamma}$	$\alpha_P^{\Gamma-\Gamma}$	$\alpha_V^{\Gamma-X}$	$\alpha_P^{\Gamma-X}$
MgTe	*B*3	−4.58	11.74	1.48	−3.79
	*B*4	−4.68	11.97		
ZnTe	*B*3	−5.00	9.03	1.25	−2.26
	*B*4	−5.12	9.26		
CdTe	*B*3	−3.07	6.67	2.24	−4.87
	*B*4	−3.21	6.95		

TABLE IV. LDA hydrostatic absolute deformation potentials (eV) of the Γ centered VBM (CBM) states of zinc-blende binary telluride semiconductors. The data of ZnTe and CdTe are taken from Ref. 31.

	α_{VBM}	α_{CBM}
MgTe	1.58	−3.00
ZnTe	0.99	−4.61
CdTe	0.89	−2.81

positive due to coupling to high-lying conduction-band states. For MgTe, as its direct ($E_g^{\Gamma-\Gamma}$) and indirect ($E_g^{\Gamma-X}$) band gaps are close in energy and their deformation potentials are of opposite sign, we find that it will turn to an indirect semiconductor when compressed hydrostatically by 4.5%.

The absolute volume-deformation potentials of the VBM and CBM states, α_{VBM} and α_{CBM}, for the $B3$ phase of MgTe are calculated using the approach described in Refs. 31 and 32. The results are shown in Table IV, with the corresponding values for ZnTe and CdTe.[31] We find that the VBM deformation potential decreases from MgTe to ZnTe to CdTe. This is because the anion p-cation d coupling in ZnTe and CdTe has a negative contribution to the VBM deformation while in MgTe, p-d coupling has opposite sign and is weak. In other words, as the material is compressed, the presence of shallow-core d states raises the VBM state. Additionally, due to the large lattice constant and longer bond length of CdTe, its VBM deformation potential is smaller than that of ZnTe. The CBM absolute deformation potentials are all negative. The large negative α_{CBM} of ZnTe is due to its small volume.

D. Band-edge alignment of zinc-blende II-VI semiconductors

The natural band alignment for the valence states of the three II-VI semiconductor compounds have been calculated using the procedure described in the previous section and the calculated absolute deformation potentials (Table IV). The corresponding natural band alignments are illustrated in Fig. 2. The conduction-band offsets can be obtained using $\Delta E_C = \Delta E_g + \Delta E_v$, where ΔE_g is the experimental band-gap difference for the zinc-blende structures.

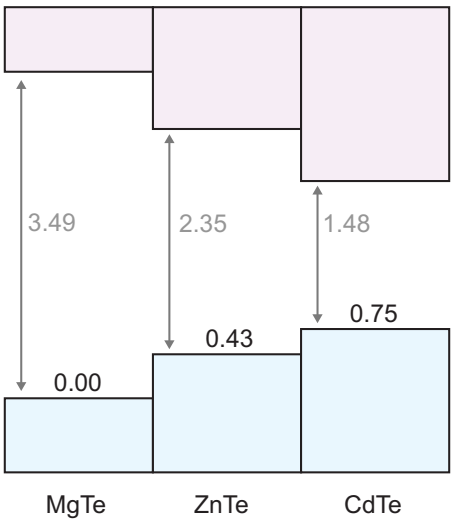

FIG. 2. (Color online) LDA-calculated natural band alignments of zinc-blende II-Te semiconductor compounds (in eV). The experimental zinc-blende band gaps (gray text) are also shown to obtain the corresponding conduction-band offsets (Ref. 9).

The VBM states increase from Mg to Zn to Cd. As there are shallow-core d levels in Zn and Cd, the anion p-cation d coupling will push their VBM high and this explains why Zn and Cd compounds have higher VBMs. Although Cd has deeper d states and weaker p-d coupling than Zn, the larger lattice constants of Cd compounds results in their higher VBM compared to the Zn compounds. These reproduce the trends previously established for II-VI semiconductors,[30] and

TABLE V. Atomic-correlation functions $\bar{\Pi}_{k,m}$ of the SQS used in our calculation at concentrations $x=0.125$, 0.25, and 0.5 and compared with the ideal values $(2x-1)^k$ of the random alloy.

	$\bar{\pi}_{2,1}$	$\bar{\pi}_{2,2}$	$\bar{\pi}_{2,3}$	$\bar{\pi}_{2,4}$	$\bar{\pi}_{3,1}$	$\bar{\pi}_{3,2}$	$\bar{\pi}_{4,1}$
$x=0.125$:							
$B3$	9/16	7/12	13/24	1/2	−7/16	−7/16	3/8
$B4$	9/16	13/24	1/2	7/12	−7/16	−19/36	3/8
$B8$	1/2	13/24	5/8	1/2	−5/12	−3/8	1/3
Random	9/16	9/16	9/16	9/16	−27/64	−27/64	81/256
$x=0.25$:							
$B3$	1/4	1/6	11/48	1/4	−1/8	−5/48	0
$B4$	1/4	1/4	1/4	1/4	−1/8	−7/36	1/8
$B8$	1/4	1/4	13/48	0	−1/8	−1/8	1/16
Random	1/4	1/4	1/4	1/4	−1/8	−1/8	1/16
$x=0.50$:							
$B3$	0	0	0	0	0	0	0
$B4$	0	0	0	−1/72	0	0	0
$B8$	0	0	0	0	0	0	0
Random	0	0	0	0	0	0	0

TABLE VI. Decomposed VD, CE, and SR contributions to the bowing parameters (in eV) of zinc-blende $A_xB_{1-x}Te$ alloys at $x=0.25$, 0.50, and 0.75.

	E_g	b_{VD}	b_{CE}	b_{SR}	b_g
		$Mg_xZn_{1-x}Te$:			
$x=0.25$	1.38	0.04	0.77	0.18	0.99
$x=0.50$	1.59	0.03	0.91	0.06	1.00
$x=0.75$	1.92	0.02	1.20	−0.20	1.02
		$Mg_xCd_{1-x}Te$:			
$x=0.25$	1.01	0.03	0.29	−0.03	0.29
$x=0.50$	1.40	0.03	0.39	−0.01	0.41
$x=0.75$	1.83	0.03	0.53	0.02	0.58
		$Zn_xCd_{1-x}Te$:			
$x=0.25$	0.72	0.33	0.09	0.00	0.42
$x=0.50$	0.85	0.35	0.10	0.01	0.46
$x=0.75$	1.03	0.38	0.10	0.05	0.53

reinforces the concept that the high VBM levels of the heavier tellurides should enhance *p*-type dopability[40] for improved semiconductor performance.

IV. TERNARY ALLOY FORMATION

The ternary random alloys $A_xB_{1-x}Te$ formed by MgTe, ZnTe, and CdTe were studied in the *B*3, *B*4, and *B*8 structures. In our calculations, we constructed five $A_xB_{1-x}Te$ SQS with $x=0.125$, 0.25, 0.50, 0.75, and 0.875 for each alloy. The structural correlation function $\bar{\Pi}_{k,m}$ for figures with k vertices and upto m neighbor distance are given in Table V, compared with the ideal random-alloy correlation functions. As can be seen, the quality of the SQSs used in our calculation is reasonable. The band-gap bowing parameter b_g of a random alloy $A_xB_{1-x}Te$, representing the quadratic deviation away from a linear interpolation of the component band gaps, was calculated according to

$$E_g^{A_xB_{1-x}Te}(x) = xE_g^{ATe} + (1-x)E_g^{BTe} - b_g x(1-x), \quad (5)$$

where E_g(ATe) and E_g(BTe) are the band gaps of ATe and BTe at their respective equilibrium lattice constants. Generally, we can decompose the formation of $A_xB_{1-x}Te$ alloys from pure ATe and BTe using a three-step process:[41] (i) for the VD contributions, we compress (or expand) ATe and BTe from their equilibrium lattice constants to the alloy lattice constant; (ii) for the charge-exchange (CE) term, we mix ATe and BTe atoms on perfect lattice sites at the alloy lattice constant; (iii) to gain the magnitude of the structural relaxation (SR), we relax all the atomic positions inside the cell using the quantum-mechanical forces. The total band-gap bowing parameter can therefore be decomposed into these three constituents, i.e., $b_g=b_{VD}+b_{CE}+b_{SR}$. The decomposed bowing parameters for the zinc-blende random alloys are listed in Table VI.

As we can see, b_g of (Mg,Zn)Te alloys or (Mg,Cd)Te alloys arise mainly from b_{CE}, as Mg has a very different electronegativity from Zn or Cd and b_g of (Zn,Cd)Te alloys are largely determined by b_{VD} due to the large lattice mismatch between ZnTe and CdTe.

TABLE VII. Alloy lattice mismatch, interaction parameters, and band-gap bowing parameters.

	Phase	$(\Delta a/\bar{a})$ %	Ω (eV)	b_g (eV)
(Mg,Zn)Te	*B*3	6.1	4.33	1.00
	*B*4	6.4	4.15	0.96
	*B*8	4.5	7.29	
(Mg,Cd)Te	*B*3	0.6	0.58	0.41
	*B*4	0.5	0.66	0.44
	*B*8	1.3	3.64	
(Zn,Cd)Te	*B*3	6.7	2.73	0.46
	*B*4	6.9	2.61	0.43
	*B*8	5.9	4.16	

The formation energy (ΔH) is defined relative to the total energy of the isostructural component phases, i.e.,

$$\Delta H = E(A_xB_{1-x}Te) - xE(ATe) - (1-x)E(BTe). \quad (6)$$

We found the formation energy is nearly a quadratic function of the composition x, i.e.,

$$\Delta H = \Omega x(1-x), \quad (7)$$

where Ω is the so-called interaction parameter. The lattice mismatch $(\Delta a/\bar{a})$, band-gap bowing parameters (b_g) and interaction parameters are listed in Table VII. As we can see, the interaction parameter Ω in the same structure decreases from (Mg,Zn)Te to (Zn,Cd)Te to (Mg,Cd)Te, indicating that both strain and chemical property (electronegativity) contribute to the formation energy but strain dominates in this system. The interaction parameters of $Mg_xCd_{1-x}Te$ alloys in the *B*3 and *B*4 structures are relatively small, suggesting that the alloys can easily form at standard growth temperature. Taking into account the larger band-gap difference between CdTe and MgTe, we propose that to increase the band gap of CdTe for solar cell application, forming $Mg_xCd_{1-x}Te$ alloys is more efficient than forming $Zn_xCd_{1-x}Te$ alloys.

The phase stability of the ternary alloys has been exam-

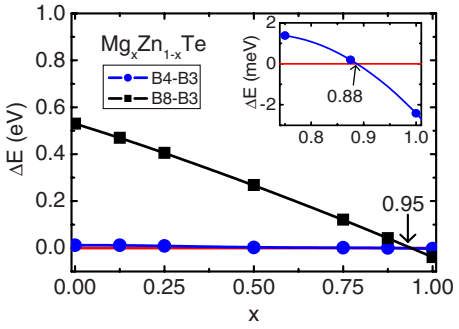

FIG. 3. (Color online) Total-energy difference per 2 atom of $Mg_xZn_{1-x}Te$ alloy in the *B*4 and *B*8 structures with respect to the *B*3 structure as a function of the composition x. The *B*3 to *B*4 transition is also shown in the inset.

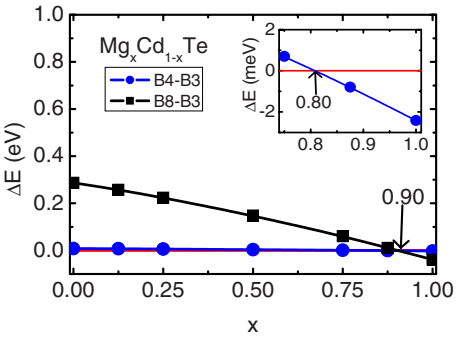

FIG. 4. (Color online) Total-energy difference per 2 atom of $Mg_xCd_{1-x}Te$ alloy in the $B4$ and $B8$ structures with respect to the $B3$ structure as a function of the composition x. The $B3$ to $B4$ transition is also shown in the inset.

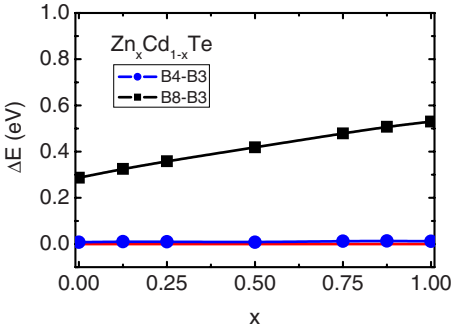

FIG. 5. (Color online) Total-energy difference per 2 atom of $Zn_xCd_{1-x}Te$ alloy in the $B4$ and $B8$ structures with respect to the $B3$ structure as a function of the composition x.

ined and the total energies of the $B4$ and $B8$ with respect to the $B3$ structures are graphed. In Fig. 3, we can see that the (Mg,Zn)Te alloy will undergo a phase transition from $B3$ to $B4$ structure at about $x=0.88$ and $x=0.95$, from $B4$ to $B8$ structure. In Fig. 4, we find that the (Mg,Cd)Te alloy will have a transition from the $B3$ to $B4$ structure at about $x=0.80$ and from the $B4$ to $B8$ structure at about $x=0.90$. Figure 5 shows that the (Zn,Cd)Te alloy will remain in the zinc-blende lattice through all Zn compositions. We also find that with all structural phase transitions to the $B8$ phase, the fundamental band gap will turn from direct to indirect along with the coordination number increase from four to six.

For most optoelectronic applications such as solar cell absorber materials, indirect band gaps should be avoided. Based on the calculated bowing parameters and the experimental band gaps of the binary tellurides, the zinc-blende (Mg,Zn)Te alloy is predicted to have an accessible direct band-gap range between 2.39 and 3.25 eV and the (Mg,Cd)Te alloy between 1.48 and 3.02 eV. Experimentally this limit has not yet been reached with epitaxial growth of the zinc-blende (Mg,Cd)Te alloy incorporating 68% Mg concentration with a band gap of 2.5 eV.[42] If transitions to the $B4$ structure are also tolerated, the accessible range can be extended by approximately 7% and 10% for the (Mg,Zn)Te and (Mg,Cd)Te alloys, respectively. As the (Zn,Cd)Te alloys are stable in the $B3$ phase over the entire compositional range, and their bowing is low, the full 1.5–2.4 eV region should be attainable.

V. CONCLUSIONS

The detailed electronic structure of MgTe, ZnTe, and CdTe and their alloys has been studied in the $B3$, $B4$, and $B8$ structures at the DFT-LDA level, which could have important applications in solid-state lighting and solar-cell devices. The band offsets between all the three binary telluride compounds have been given using the new approach, by taking into account the core-level deformation. The bowing parameters of the alloys were calculated and were used to predict band gaps of the ternary alloy systems which can be directly compared with experiment. The stability of ternary alloys were studied, and with the calculated bowing parameters, the zinc-blende (Mg,Zn)Te [(Mg,Cd)Te] alloys are predicted to be stable with less than 88% (80%) Mg content with direct alloy band gaps between 2.39 (1.48)eV and 3.25 (3.02)eV. The (Zn,Cd)Te zinc-blende alloy is stable over the full compositional range.

ACKNOWLEDGMENTS

The work at Fudan University is partially supported by the National Science Foundation of China, the Special Funds for Major State Basic Research, and the project of MOE and Shanghai Municipality. The computation is performed in the Supercomputer Center of Shanghai, the Supercomputer Center of Fudan University, and CCS. The work at NREL is funded by the U.S Department of Energy (DOE), under Contract No. DE-AC36-08GO28308, which employed computing resources of the National Energy Research Scientific Computing Center supported by DOE under Contract No. DE-AC02-05CH11231.

[1] M. Jaros, Rep. Prog. Phys. **48**, 1091 (1985).
[2] J. E. Bernard, L. G. Ferreira, S.-H. Wei, and A. Zunger, Phys. Rev. B **38**, 6338 (1988).
[3] C. Y. Moon, S.-H. Wei, Y. Z. Zhu, and G. D. Chen, Phys. Rev. B **74**, 233202 (2006).
[4] S. Chen, X. G. Gong, A. Walsh, and S.-H. Wei, Appl. Phys. Lett. **94**, 041903 (2009).
[5] M. Sanati, G. L. W. Hart, and A. Zunger, Phys. Rev. B **68**, 155210 (2003).
[6] Y. Z. Zhu, G. D. Chen, H. Ye, A. Walsh, C. Y. Moon, and S.-H. Wei, Phys. Rev. B **77**, 245209 (2008).
[7] S.-H. Wei, S. B. Zhang, and A. Zunger, J. Appl. Phys. **87**, 1304 (2000).
[8] A. Walsh and S.-H. Wei, Phys. Rev. B **76**, 195208 (2007).
[9] O. M. Madelung, *Semiconductors: Data Handbook*, 3rd ed. (Springer, Berlin, 2004).

[10] A. Shah, P. Torres, R. Tscharner, N. Wyrsch, and H. Keppner, Science **285**, 692 (1999).
[11] L. L. Kazmerski, F. R. White, and G. K. Morgan, Appl. Phys. Lett. **29**, 268 (1976).
[12] K. Mitchell, A. L. Fahrenbruch, and R. H. Bube, J. Vac. Sci. Technol. **12**, 909 (1975).
[13] M. W. Wang, M. C. Phillips, J. F. Swenberg, E. T. Yu, J. O. McCaldin, and T. C. McGill, J. Appl. Phys. **73**, 4660 (1993).
[14] M. W. Wang, J. F. Swenberg, M. C. Phillips, E. T. Yu, J. O. McCaldin, R. W. Grant, and T. C. McGill, Appl. Phys. Lett. **64**, 3455 (1994).
[15] W. Klemm and K. Wahl, Z. Anorg. All. Chem. **266**, 289 (1951).
[16] A. Kuhn, A. Chevy, and M. J. Naud, J. Cryst. Growth **9**, 263 (1971).
[17] S. G. Parker, A. R. Reinberg, J. E. Pinnell, and W. C. Holton, J. Electrochem. Soc. **118**, 979 (1971).
[18] C.-Y. Yeh, Z. W. Lu, S. Froyen, and A. Zunger, Phys. Rev. B **45**, 12130 (1992).
[19] C.-Y. Yeh, Z. W. Lu, S. Froyen, and A. Zunger, Phys. Rev. B **46**, 10086 (1992).
[20] T. Li, H. Luo, R. G. Greene, A. L. Ruoff, S. S. Trail, and F. J. DiSalvo, Jr., Phys. Rev. Lett. **74**, 5232 (1995).
[21] W. Kohn and L. J. Sham, Phys. Rev. **140**, A1133 (1965).
[22] P. Hohenberg and W. Kohn, Phys. Rev. **136**, B864 (1964).
[23] D. M. Ceperley and B. J. Alder, Phys. Rev. Lett. **45**, 566 (1980).
[24] G. Kresse and J. Furthmüller, Phys. Rev. B **54**, 11169 (1996).
[25] G. Kresse and J. Furthmüller, Comput. Mater. Sci. **6**, 15 (1996).
[26] G. Kresse and D. Joubert, Phys. Rev. B **59**, 1758 (1999).
[27] H. J. Monkhorst and J. D. Pack, Phys. Rev. B **13**, 5188 (1976).
[28] F. D. Murnaghan, Proc. Natl. Acad. Sci. U.S.A. **30**, 244 (1944).
[29] S. P. Kowalczyk, J. T. Cheung, E. A. Kraut, and R. W. Grant, Phys. Rev. Lett. **56**, 1605 (1986).
[30] S.-H. Wei and A. Zunger, Appl. Phys. Lett. **72**, 2011 (1998).
[31] Y. H. Li, X. G. Gong, and S.-H. Wei, Phys. Rev. B **73**, 245206 (2006).
[32] Y. H. Li, X. G. Gong, and S.-H. Wei, Appl. Phys. Lett. **88**, 042104 (2006).
[33] S.-H. Wei, L. G. Ferreira, J. E. Bernard, and A. Zunger, Phys. Rev. B **42**, 9622 (1990).
[34] A. Zunger, S.-H. Wei, L. G. Ferreira, and J. E. Bernard, Phys. Rev. Lett. **65**, 353 (1990).
[35] L. Vegard, Z. Phys. **5**, 17 (1921).
[36] S.-H. Wei and A. Zunger, Phys. Rev. B **37**, 8958 (1988).
[37] B. K. Agrawal and S. Agrawal, Phys. Rev. B **45**, 8321 (1992).
[38] G. M. Dalpian, Y. Yan, and S.-H. Wei, Appl. Phys. Lett. **89**, 011907 (2006).
[39] S.-H. Wei and A. Zunger, Phys. Rev. B **60**, 5404 (1999).
[40] S. B. Zhang, S.-H. Wei, and A. Zunger, Phys. Rev. Lett. **84**, 1232 (2000).
[41] J. E. Bernard and A. Zunger, Phys. Rev. B **34**, 5992 (1986).
[42] A. Waag, H. Heinke, S. Scholl, C. R. Becker, and G. Landwehr, J. Cryst. Growth **131**, 607 (1993).